J. Mol. Model. **1999**, *5*, 196 – 202

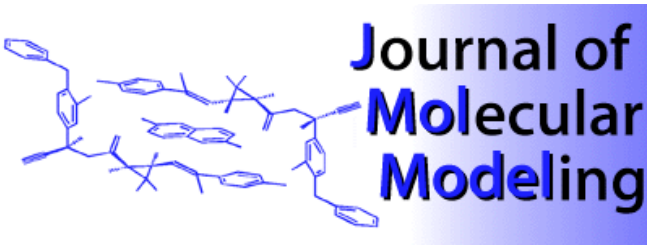

FULL PAPER

© Springer-Verlag 1999

Novel Zinc Protein Molecular Dynamics Simulations: Steps Toward Antiangiogenesis for Cancer Treatment

Yuan-Ping Pang

Mayo Clinic Cancer Center, Tumor Biology Program, Department of Pharmacology, Molecular Neuroscience Program Mayo Foundation for Medical Education and Research, 200 First Street SW, Rochester, MN 55905, USA. E-mail: pang@mayo.edu

Received: 30 June 1999/ Accepted: 3 September 1999/ Published: 19 October 1999

Abstract Angiogenesis is the formation of new blood vessels induced by tumors as a lifeline for oxygen and nutrients and as exits for spread of cancer cells. Blocking tumors' blood supply could starve tumors thus saving cancer patients, and is termed antiangiogenesis. Matrix metalloproteinases (MMPs) are a class of proteins containing Zn^{2+} in the active site that cleave the constituents of the extracellular matrix and control angiogenesis. Selective inhibitors of MMPs therefore hold promise in antiangiogenesis for treating cancers, but development of such inhibitors is currently hampered by a paucity of effective computational methods for evaluating the intermolecular interactions between zinc and its coordinates and for performing nanosecond length molecular dynamics simulation of zinc proteins. Here I report an approach for simulating the four-coordinate zinc complex in proteins without use of covalent bonds or harmonic restraints applied to the zinc complex. This approach uses four cationic dummy atoms tetrahedrically placed around the zinc nucleus to mimic zinc's $4s4p^3$ vacant orbitals that accommodate lone-pair electrons of the zinc coordinates thus imposing the orientational requirement for the zinc coordinates and simulating zinc's propensity to a tetrahedral coordination geometry. It hence permits evaluating binding free energy of zinc coordinates and simulating the exchanges of zinc's ambidentate coordinates in proteins, and is expected to expedite the search of effective angiogenesis inhibitors to combat cancers.

Keywords Force field parameters, Endostatin, Matrix metalloproteinases, Carbonic anhydrase, Carboxypeptidase A

Running title Zinc Protein Molecular Dynamics Simulations

Introduction

Angiogenesis is the formation of new blood vessels induced by tumors as a lifeline for oxygen and nutrients and as exits for spreading cancer cells. Blocking the tumors' blood supply could starve tumors, thus saving cancer patients, and is termed antiangiogenesis [1]. Matrix metalloproteinases (MMPs) are a class of proteins containing Zn^{2+} in the active site that cleave the constituents of the extracellular matrix and control angiogenesis [2,3]. Selective inhibitors of MMPs therefore hold promise in antiangiogenesis for treating can-

Table 1 *The bonded parameters of the tetrahedral zinc divalent cation (ZN = Zn^{2+} and DZ = dummy atom, for the nonbonded parameters see Figure 1)*

Bond	**K [kcal·mol^{-1}·Å^{-2}]**	**R_{eq} [Å]**		
DZ-ZN	540.0	0.90		
DZ-DZ	540.0	1.47		
Angle	**K [kcal·mol^{-1}·radian^{-2}]**	**T_{eq} [deg.]**		
DZ-ZN-DZ	55.0	109.50		
DZ-DZ-DZ	55.0	60.00		
DZ-DZ-ZN	55.0	35.25		
Torsion	**IDIVF**	**$V_n/2$ [kcal·mol^{-1}]**	**γ [deg.]**	**n**
ZN-DZ-DZ-DZ	1	0.0	35.3	2.0
DZ-ZN-DZ-DZ	1	0.0	120.0	2.0
DZ-DZ-DZ-DZ	1	0.0	70.5	2.0

cers, but development of such inhibitors is currently hampered by a paucity of effective computational methods for evaluating the intermolecular interactions between zinc and its coordinates and for performing nanosecond length molecular dynamics (MD) simulation of zinc proteins.

Two general methods have been reported for zinc protein MD simulations. The first one, termed the *bonded* model, uses covalent bonds between zinc and its coordinates to maintain the polyhedral zinc coordination geometry in proteins during MD simulations [4-6]. Use of such covalent bonds prevents one from evaluating the intermolecular interactions between zinc and its coordinates and from simulating the exchanges of the zinc coordinates. The second one termed *nonbonded* model [7-9] maintains zinc's polyhedral geometry with the electrostatic and van der Waals forces instead. However, in our nanosecond length MD simulations of zinc-containing farnesyltransferase employing the Particle Mesh Ewald (PME) method [10] to calculate the long-range electrostatic interactions, the four-coordinate (tetrahedral) zinc complex identified in the X-ray structure of farnesyltransferase was always changed to a six-coordinate (octahedral) zinc complex despite exhaustive efforts using different force field parameters of the zinc divalent cation developed within the paradigm of the *nonbonded* model. Technically, the tetrahedron-to-octahedron problem was caused by the force field parameters of the zinc ion that were developed with a zinc ion coordinating to six water molecules [8]. Using such parameters, a tetrahedral zinc complex will inevitably be converted to an octahedral complex if the tetrahedral complex is exposed to water long enough in an MD simulation. Conceptually, this problem is due to the simplification that zinc's coordination geometry is solely determined by the repulsion among the zinc coordinates (*vide infra*). Although both methods are useful in many cases, the limitations of the two methods described here have hampered the use of computational approaches in the search of effective angiogenesis inhibitors.

Results

To develop an effective method for zinc protein MD simulations, we have recently surveyed zinc protein crystal structures and reported the inherent uncertainty in classifying zinc's five- and six-ligand coordination patterns in proteins due to the experimental resolutions [11]. We have accordingly proposed that the zinc divalent cation coordinates to only four coordinates [11]. This is mainly because of its electronic structure that energetically favorably accommodates four pairs of electrons in its vacant $4s4p^3$ orbitals. In other words, zinc's coordination geometry is determined mainly by its electronic

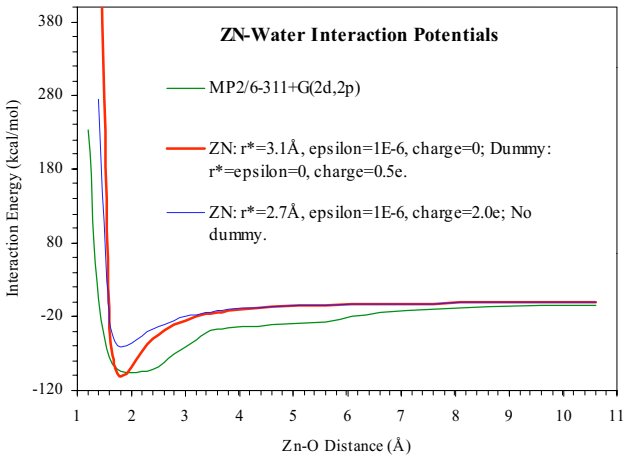

Figure 1 *The zinc-water interaction potentials obtained from the quantum mechanics calculations (*green*) and from the molecular mechanics calculations with* the tetrahedral zinc divalent cation *(*red*) and with the conventional zinc divalent cation (*blue*). Zn^{2+} and the cationic dummy atom are abbreviated as ZN and dummy, respectively.*

Table 2 *Nonbonded distances (Å) calculated from the structures of the 2.0 ns MD simulations and the X-ray structures.*

	average ± deviation (no.)	
	MD structure	**X-ray structure**
Carboxypeptidase A[a]		
Zn-OW (Wat^{571})	1.9 ± 0.03 (2000)	2.0 ± 0.1 (8)
Zn-ND1 (H^{69})	2.1 ± 0.04 (2000)	2.1 ± 0.07 (13)
Zn-ND1 (H^{196})	2.1 ± 0.04 (2000)	2.1 ± 0.05 (13)
Zn-OE1 (E^{72})	2.2 ± 0.3 (2000)	2.2 ± 0.09 (13)
Zn-OE2 (E^{72})	2.6 ± 0.5 (2000)	2.3 ± 0.2 (13)
Zn-CD (E^{72})	2.8 ± 0.1 (2000)	2.6 ± 0.09 (12)
Zn-OH (Y^{248})	17.7 ± 0.7 (2000)	19.1 ± 0.8 (3)
Zn-OE1 (E^{270})	5.4 ± 0.9 (2000)	4.7 ± 0.1 (3)
Zn-OE2 (E^{270})	5.2 ± 1.0 (2000)	4.1 ± 0.06 (3)
Zn-CD (E^{270})	5.6 ± 0.6 (2000)	4.9 ± 0.06 (3)
OW-OE1 (Wat^{571}, E^{270})	4.1 ± 0.8 (2000)	3.3 ± 0.1 (3)
OW-OE2 (Wat^{571}, E^{270})	4.0 ± 1.0 (2000)	2.6 ± 0.1 (3)
OW-OH (Wat^{571}, Y^{248})	16.1 ± 0.7 (2000)	17.6 ± 0.8 (3)
Carbonic anhydrase II[b]		
Zn-OW (Wat^{263})	1.9 ± 0.02 (2000)	2.1 ± 0.1 (17)
Zn-NE2 (H^{94})	2.0 ± 0.03 (2000)	2.1 ± 0.1 (34)
Zn-NE2 (H^{96})	2.0 ± 0.03 (2000)	2.1 ± 0.08 (34)
Zn-ND1 (H^{119})	2.0 ± 0.04 (2000)	2.0 ± 0.1 (34)
Zn-NE2 (H^{64})	8.1 ± 0.7 (2000)	8.6 ± 1.2 (31)
Zn-CD (E^{106})	4.5 ± 0.6 (2000)	4.9 ± 0.06 (34)
Zn-OE1 (E^{106})	4.9 ± 1.0 (2000)	5.5 ± 0.09 (34)
Zn-OE2 (E^{106})	3.9 ± 0.6 (2000)	4.0 ± 0.09 (34)
Zn-CD (E^{117})	6.7 ± 0.2 (2000)	7.0 ± 0.1 (31)
Zn-OE1 (E^{117})	7.0 ± 0.4 (2000)	7.8 ± 0.1 (31)
Zn-OE2 (E^{117})	6.5 ± 0.2 (2000)	6.6 ± 0.07 (31)
Zn-OG1 (T^{199})	4.4 ± 0.4 (2000)	3.8 ± 0.1 (34)
Zn-OG1 (T^{200})	7.2 ± 0.5 (2000)	6.2 ± 0.2 (33)
Rubredoxin[c]		
Zn-SG (C^{6})	2.1 ± 0.04 (2000)	2.4 ± 0.5 (1)
Zn-SG (C^{9})	2.1 ± 0.04 (2000)	2.3 ± 0.5 (1)
Zn-SG (C^{39})	2.1 ± 0.04 (2000)	2.4 ± 0.5 (1)
Zn-SG (C^{42})	2.1 ± 0.04 (2000)	2.3 ± 0.5 (1)

[a] The X-ray structures of carboxypeptidase A with resolutions higher than or equal to 2.0 Å include 5cpa, 6cpa, 1aye, 7cpa, 1bav, 8cpa, 1cbx, 3cpa, 1cpx, 1pca, 1yme, 2ctb, and 2ctc.

[b] The X-ray structures of carbonic anhydrase II with resolutions higher than or equal to 2.0 Å include 1ave, 1bcd, 1bic, 1bv3, 1cao, 1cil, 1cng, 1cni, 1cnj, 1cra, 1hea, 1heb, 1hec, 1hed, 1mua, 1ray, 1raz, 1uga, 1ugb, 1ugc, 1ugd, 1uge, 1ugf, 2cbd, 1ydb, 1ydc, 3ca2, 2ca2, 1ca2, 1zsb, 1zsc, 2cba, 2cbb, and 2cbc.

[c] The deviation of the nonbonded distance in the structure of 1irn was estimated from $\sqrt{(B_i + B_j)/(8\pi^2)}$, *where* B_i *and* B_j *are the B values of atoms i and j, respectively.*

structure and not by the repulsion among the zinc coordinates. Experimental observations of the five- and six-coordinate complexes were due to one or two pairs of ambidentate coordinates that exchanged over time and were averaged as bidentate coordinates [11]. We have also performed *ab initio* calculations of proton dissociation energies of common zinc coordinates and reasoned that, just like thiolate [12] and the deprotonated peptide nitrogen atom [13], histidine is deprotonated as anionic histidinate when coordinating to Zn^{2+} in proteins [14].

Accordingly, I have devised a method, termed the *cationic dummy atom* model, for simulating zinc proteins with two critical attributes. The first is to replace Zn^{2+} with a five-atom molecule termed *tetrahedral zinc divalent cation* to effectively maintain the tetrahedral zinc complex in MD simulations. The second is to deprotonate all zinc coordinates, namely, using thiolate, imidazolate, carboxylate, and hydroxide as zinc coordinates in proteins.

To construct the *tetrahedral zinc divalent cation*, four identical dummy (pseudo) atoms are placed at the four apices of a tetrahedron with the zinc nucleus located at the center of the tetrahedron. The dummy atoms are covalently bonded to the zinc nucleus with the bonded parameters developed within the framework of the AMBER 95 force field [15] (Table 1). The zinc nucleus is assigned only with the van der Waals parameters (i.e., r* = 3.1 Å, ε = 1E-6 kcal·mol^{-1}, and q = 0), while the dummy atom is assigned only with charge (i.e., r* = ε = 0, and q = 0.5 e). The four cationic atoms are dummy in a sense that they do not sterically interact with other atoms, but they represent zinc's four vacant $4s4p^3$ orbitals, thus imposing the orientational requirement for the zinc coordinates and simulating zinc's propensity to a tetrahedral coordination geometry. Energy minimizations of highly distorted zinc-

Table 3 *Angles (deg. of arc) calculated from the structures of the 2.0 ns MD simulations and the X-ray structures.*

[a] The X-ray structures of carboxypeptidase A with resolutions higher than or equal to 2.0 Å include 5cpa, 6cpa, 1aye, 7cpa, 1bav, 8cpa, 1cbx, 3cpa, 1cpx, 1pca, 1yme, 2ctb, and 2ctc.
[b] The X-ray structures of carbonic anhydrase II with resolutions higher than or equal to 2.0 Å include 1ave, 1bcd, 1bic, 1bv3, 1cao, 1cil, 1cng, 1cni, 1cnj, 1cra, 1hea, 1heb, 1hec, 1hed, 1mua, 1ray, 1raz, 1uga, 1ugb, 1ugc, 1ugd, 1uge, 1ugf, 2cbd, 1ydb, 1ydc, 3ca2, 2ca2, 1ca2, 1zsb, 1zsc, 2cba, 2cbb, and 2cbc.
[c] The angle deviation in the structure of 1irn was estimated from atan(ΔD/D), where ΔD is the deviation of the SG-Zn distance (0.5 Å) and D is the SG-Zn distance (2.4 Å).

	average ± deviation (no.)	
	MD structures	**X-ray structures**
Carboxypeptidase A [a]		
OW^{571}-Zn-$OE1^{72}$	120 ± 8 (2000)	118 ± 8 (6)
OW^{571}-Zn-$ND1^{69}$	108 ± 4 (2000)	114 ± 9 (6)
OW^{571}-Zn-$ND1^{196}$	107 ± 4 (2000)	104 ± 10 (6)
$OE1^{72}$-Zn-$ND1^{69}$	123 ± 5 (2000)	120 ± 7 (14)
$OE1^{72}$-Zn-$ND1^{196}$	88 ± 3 (2000)	95 ± 7 (14)
$ND1^{69}$-Zn-$ND1^{196}$	102 ± 4 (2000)	100 ± 4 (14)
OW^{571}-Zn-$OE2^{72}$	101 ± 8 (2000)	92 ± 5 (6)
$OE2^{72}$-Zn-$ND1^{69}$	99 ± 11 (2000)	99 ± 11 (14)
$OE2^{72}$-Zn-$ND1^{196}$	136 ±16 (2000)	149 ± 8 (14)
Carbonic anhydrase II [b]		
OW^{263}-Zn-$NE2^{94}$	111 ± 4 (2000)	105 ± 5 (16)
OW^{263}-Zn-$NE2^{96}$	108 ± 4 (2000)	113 ± 4 (16)
OW^{263}-Zn-$ND1^{119}$	107 ± 4 (2000)	114 ± 4 (16)
$NE2^{94}$-Zn-$NE2^{96}$	109 ± 4 (2000)	107 ± 3 (34)
$NE2^{94}$-Zn-$ND1^{119}$	115 ± 4 (2000)	114 ± 3 (34)
$NE2^{96}$-Zn-$ND1^{119}$	106 ± 4 (2000)	102 ± 3 (34)
Rubredoxin [c]		
SG^{6}-Zn-SG^{9}	106 ± 4 (2000)	113 ± 12 (1)
SG^{6}-Zn-SG^{39}	114 ± 4 (2000)	112 ± 12 (1)
SG^{6}-Zn-SG^{42}	110 ± 4 (2000)	105 ± 12 (1)
SG^{9}-Zn-SG^{39}	109 ± 4 (2000)	104 ± 12 (1)
SG^{9}-Zn-SG^{42}	110 ± 4 (2000)	112 ± 12 (1)
SG^{39}-Zn-SG^{42}	107 ± 4 (2000)	112 ± 12 (1)

containing protein structures can sometimes cause drastic deformations of the geometry of the *tetrahedral zinc divalent cation*. However, this can be avoided by introducing covalent bonds between the dummies with the parameters listed in Table 1. An alternative approach is to energy minimize the highly energetic structure with harmonic restraints applied to the *tetrahedral zinc divalent cation* and its coordinates followed by an energy minimization without the harmonic restraints.

The *cationic dummy atom* model uses the deprotonated carboxylate group of Asp and Glu, thiolate, imidazolate and hydroxide in the first zinc coordination shell, and the protonated carboxylate group of Asp and Glu in the second zinc coordination shell when it forms a hydrogen bond with the first-shell coordinates directly or indirectly via a water molecule or the hydroxyl group of Ser or Thr serving as a relay.

To minimize the difference of the zinc solvation free energy between the calculated and experimental values due to the under-evaluation of zinc's interaction energy inherited from the additive force field that can not effectively address the polarization of the zinc complex, the van der Waals radius of the zinc nucleus of the *tetrahedral zinc divalent cation* was shortened to 3.1 Å in order to strengthen the interaction of the zinc ion with its coordinates. This value caused a reduction of the Zn-S distance by 0.2 Å in MD simulations compared to the average Zn-S distance (2.3 ± 0.1 Å) obtained from our survey of zinc protein crystal structures [11]. However, the calculated zinc solvation energy was improved to -448 kcal·mol^{-1}, which is about 8% smaller than the experimental measurement of -485 kcal·mol^{-1} [16]. The force field parameters of the *tetrahedral zinc divalent cation* thus represent a balance between the zinc coordinate distances and the zinc coordinate interaction energies in MD simulations. As indicated in Figure 1, the interaction surface obtained from the *ab initio* calculations employing the Gaussian 94 program [17] reveals a flat region (the Zn-O distance ranges from 1.8 to 2.0 Å) where a minimal energy (maximal association energy) of -94.6 kcal·mol^{-1} can be obtained; the interaction surface derived from the molecular mechanics calculations using the *tetrahedral zinc divalent cation* gives a minimal energy of –103.0 kcal·mol^{-1} at the Zn-O distance of 1.8 Å, whereas the interaction surface derived from the molecular mechanics calculations with the traditional zinc divalent cation yields a minimum of –61.5 kcal·mol^{-1} at the same Zn-O distance. Clearly, use of the *tetrahedral zinc divalent cation* significantly alleviates the problem of the under-evaluation of zinc's interaction energy inherited from the additive molecular mechanics force field.

The practicality of the *cationic dummy atom* model is demonstrated by the MD simulations of carbonic anhydrase (PDB code: 1ca2), carboxypeptidase A (PDB code: 5cpa) and rubredoxin (PDB code: 1irn) in water at 25 °C. These pro-

Table 4 *Root mean square deviations (RMSDs) between the X-ray structure and the structures (excluding H, Na^+ and Cl^- atoms) averaged over a 2.0 ns MD simulation.*

protein (resolution, Å)	RMSD, Å (No. of matched atoms) overlay the entire protein		overlay the zinc complex	
	zinc complex	entire protein	zinc complex	entire protein
1ca2 (2.00)	0.74 (36)	1.28 (2045)	0.34 (36)	2.89 (2045)
5cpa (1.54)	0.34 (35)	1.09 (2442)	0.20 (35)	1.33 (2442)
1irn (1.20)	0.52 (29)	1.21 (417)	0.42 (29)	1.34 (417)

teins represent the three most populated zinc-coordinate compositions found in our zinc protein survey [11]. First, for the three proteins, the zinc tetrahedral geometry was retained well during all of our 2.0 ns MD simulations. This is evident from the average distances between the zinc ion and its coordinates (Table 2) and the average angles between the zinc coordinates (Table 3) compared to the values measured in the X-ray structures. On the contrary, the tetrahedral zinc complex was converted to a trigonal bipyramidal zinc complex during the 1.0 ns simulations of carbonic anhydrase using different force field parameters of zinc developed within the paradigm of the *nonbonded* model. Second, the three protein structures bound with the *tetrahedral zinc divalent cation* did not diverge from the X-ray structures during all of our 2.0 ns MD simulations. This is evident from the root mean square deviations of the non-hydrogen atoms in the X-ray structure and in the average structure of a 2.0 ns MD simulation (Table 4) and the nonbonded distances in comparison with the values obtained from the X-ray structures (Table 2). Furthermore, the structures, nonbonded distances and angles averaged over a 2.0 ns MD simulation are almost identical to the ones averaged over a 1.0 ns MD simulation (data not shown). Lastly and most importantly, use of the *tetrahedral zinc divalent cation* confers a simulation of the exchange of zinc's ambidentate coordinates. As depicted in Figure 2, where the Zn-O distances close to 2.0 Å reflect that the oxygen atom coordinates to the zinc ion, the two oxygen atoms (OE1 and OE2) of the carboxylate group of Glu72 alternately coordinate to Zn^{2+} in the 2.0 ns simulation of carboxypeptidase A bound with the *tetrahedral zinc divalent cation*. It is worth noting that Glu72 is a bidentate coordinate in the structure averaged over the 2.0 ns MD simulation (Table 2), but it is an ambidentate coordinate in all the instantaneous structures in the 2.0 ns MD simulation (Figure 2). This observation is consistent with our rationale that the experimental observations of the five- and six-coordinate complexes of zinc are due to one or two ambidentate coordinates that exchange over time and are averaged as bidentate coordinates [11]. The ability of the *cationic dummy atom* model to simulate the exchanges of zinc's ambidentate ligands described here advances the understanding of the nature of zinc coordination in proteins, and enables proper evaluations of thermodynamic quantities such as free energy of binding contributed by the conformational fluctuations of the zinc-binding site. Furthermore, it offers a means to refine the X-ray structures of zinc proteins in which only one oxygen atom of a carboxylate group can coordinate to zinc, but the resolutions of the crystallographic studies are not high enough to determine which of the two

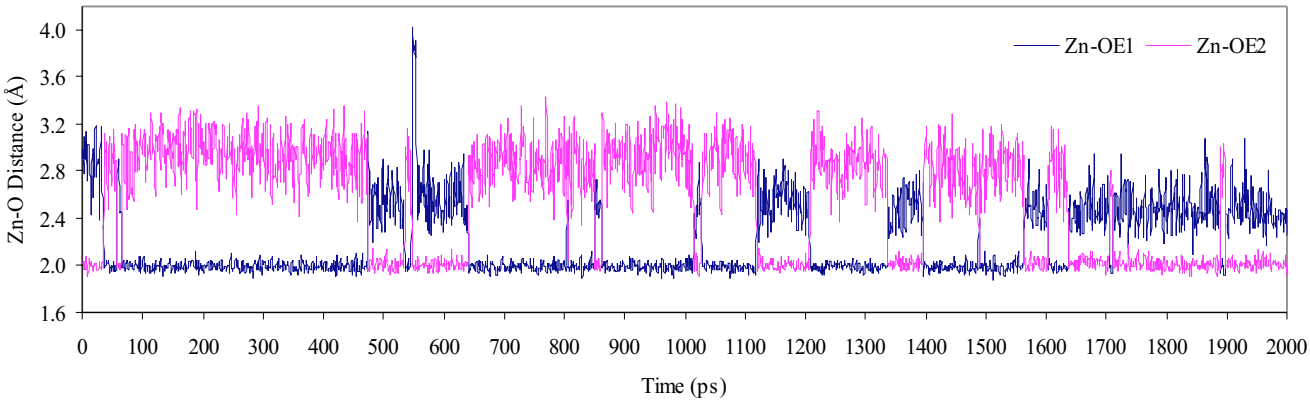

Figure 2 *The simulation of the exchange of the two oxygen atoms (OE1 and OE2) of the carboxylate group of Glu72 in carboxypeptidase A as zinc's ambidentate coordinates (The Zn-OE1(2) distances were calculated from the trajectories saved at 1.0 ps intervals by employing the CARNAL module of the AMBER 5.0 program).*

Table 5 *The RESP charges of histidinate and hydroxide (for definitions of the atom names see ref [15])*

atom name	charge	atom name	charge
	hisdidinate		
N	-0.5641	ND1	-0.7626
H	0.2469	CE1	0.4994
CA	0.3171	HE1	-0.0295
HA	0.0096	NE2	-0.7656
CB	-0.1347	CD2	0.0405
HB2	0.0083	HD2	0.0525
HB3	0.0381	C	0.4588
CG	0.1504	O	-0.5653
	hydroxide		
HO	0.2049	OH	-1.2049

oxygen atoms of the carboxylate group should coordinate to zinc. Similarly, it offers a means to refine the NMR structures of zinc proteins.

Conclusion

Much of the progress in antiangiogenesis relies on development of effective angiogenesis inhibitors. The zinc protein MD simulation approach reported here is expected to facilitate the search of effective angiogenesis inhibitors for treating cancers. Indeed, the *cationic dummy atom* model has already been successfully used in our farnesyltransferase inhibitor search [18] and in our MD simulations of endostatin, one of the most potent angiogenesis inhibitors [19], to evaluate the conformational stability of endostatin and to design improved mimetics.

Methods

All the MD simulations were performed by employing the SANDER module of the AMBER 5.0 program [20] with the Cornell et al. force field and additional parameters in Tables 1 and 5 and in Figure 1 according to a slightly modified literature procedure [21]. The values of the keywords in the uppercase letters used by the AMBER program are described in parentheses. All the MD simulations used 1) the SHAKE procedure for all the covalent bonds of the system (NTC = 3 and NTF = 3) [22]; 2) a time step of 1.0 fs; 3) a dielectric constant $\varepsilon = 1.0$; 4) the Berendsen coupling algorithm (NTT = 1) [23]; 5) the PME method [10] used to calculate the electrostatic interactions (see below for details); 6) a nonbonded atom-pair list updated at every 20 steps; 7) a distance cutoff of 8.0 Å used to calculate the nonbonded interactions; and 8) the default values of all other keywords not specified here. Each protein structure was simulated in a TIP3P [24] water box with a periodic boundary condition at constant temperature and pressure (NCUBE = 20, QH = 0.4170, DISO = 2.20, DISH = 2.00, CUTX = CUTY = CUTZ = 8.2, NTB = 2, TEMP0 = 298, PRES0 = 1.0, and NTP = 1). The resulting system was first energy minimized for 500 steps in order to remove close van der Waals contacts of the system. The energy minimized system was then slowly heated to 298 K (10K/ps and NTX = 1) and equilibrated for 50 ps before simulation. A weak harmonic restraint in the Cartesian space (NTR = 1 and the harmonic potential force constant = 0.01 kcal·mol^{-1}) was applied to the counter ions added to neutralize the system and the water molecules determined by the crystallographic analysis in order to avoid large separations of these small molecules from the protein during nanosecond length MD simulations, which could occasionally cause simulation crash. The location of each counter ion described below was determined by energy minimization with a positional constraint applied to all the atoms except for the counter ion.

The zinc solvation free energies were calculated by using the GIBBS module of the AMBER 5.0 program according to a literature procedure [21]. A distance cutoff of 15.0 Å was used for calculating the nonbonded steric and electrostatic interactions. *The tetrahedral zinc divalent cation* was solvated in a TIP3P water box with a periodic boundary condition (NCUBE = 20, QH = 0.4170, DISO = 2.20, DISH = 2.00, CUTX=CUTY=CUTZ=15.5, NTB = 2, TEMP0 = 298, PRES0 = 1.0, and NTP = 1). The zinc solvation free energy was computed along two different perturbation paths, and included the Born correction, which partly accounts for the error introduced by the use of a finite truncation for the electrostatic interaction. The first perturbation path perturbed the *tetrahedral zinc divalent cation* directly to null during a 1.0 ns MD simulation. The second perturbed the *tetrahedral zinc divalent cation* to methane that was then perturbed to null during a 2.0 ns MD simulation. The difference in solvation energy between the two paths is 0.8 kcal·mol^{-1}, indicating that the calculated solvation energies were converged.

The RESP charges of histidinate and hydroxide were derived by using the Gaussian 94 program [17] and the AMBER 5.0 program according to a literature procedure [25]. The charges of histidinate were averaged from the charges of two histidinates with different populated side-chain conformations [25].

Simulation of Carbonic Anhydrase

All the Glu and Asp residues were deprotonated except for Glu106 and Glu117. All the Arg and Lys residues, His4, His10, His36, His107 and Cys206 were protonated. His15, His17 and His64 were assigned as the HIE (N^{ε}-H) tautomer except for His122 as the HID (N^{δ}-H) tautomer. His94, His96, His119 and H_2O265 were treated as histidinate and hydroxide, respectively. Lys24, Arg27, Lys39, Asp72, Glu221, and Arg246 were each neutralized by adding a counter ion (Na^+ or Cl^-), respectively. The parameters for the PME method were de-

fined as follows: BOXX=72.3387, BOXY=66.2812, BOXZ=62.7392, α=β=γ=90.0, NFFTX=64, NFFTY=64, NFFTZ=64, SPLINE_ORDER=4, ISCHARGED=0, EXACT_EWALD=0, DSUM_TOL=0.00001.

Simulation of Carboxypeptidase A

All the Glu and Asp residues were deprotonated except for Asp142 and Glu270. All the Arg and Lys residues, His13, His29, His120, and His303 were protonated. His186 and His166 were assigned as HIE and HID, respectively. His69, His196, and H_2O313 were treated as histidinate and hydroxide, respectively. Lys85, Arg124, Lys190, Lys231, Lys239, Lys224 and Glu302 were each neutralized by adding a counter ion (Na^+ or Cl^-), respectively. The parameters for the PME method were defined as follows: BOXX=76.5983, BOXY=71.4923, BOXZ=67.0672, α=β=γ=90.0, NFFTX=64, NFFTY=64, NFFTZ=64, SPLINE_ORDER=4, ISCHARGED=1, EXACT_EWALD=0, DSUM_TOL=0.00001.

Simulation of Rubredoxin

All the Glu, Asp and Cys residues were deprotonated while all the Lys residues were protonated. Asp21, Asp36, Asp17, Asp19, Asp35, Asp47, Glu50, Glu53, were each neutralized by adding a counter ion (Na^+), respectively. The parameters for the PME method were defined as follows: BOXX=46.8357, BOXY=44.5514, BOXZ=40.6069, ALPHA=BETA=GAMMA=90.0, NFFTX=49, NFFTY=49, NFFTZ=49, SPLINE_ORDER=4, ISCHARGED=0, EXACT_EWALD=0, DSUM_TOL=0.00001.

Acknowledgement The author acknowledges the support by the Mayo Foundation for Medical Education and Research.

Supplementary material available 1) Topology files of the tetrahedral zinc divalent cation, histidinate, and hydroxide are available in AMBER 5.0 format. 2) A force field parameter file (0196frc.txt) for the tetrahedral zinc divalent cation is given in AMBER 5.0 format.

References

1. Folkman, J. *N. Eng. J. Med.* **1971**, *285*, 1182.
2. Hanahan, D.; Folkman, J. *Cell* **1996**, *86*, 353.
3. Vu, T. H.; Shipley, J. M.; Bergers, G.; Berger, J. E.; Helms, J. A.; Hanahan, D.; Shapiro, S. D.; Senior, R. M.; Werb, Z. *Cell* **1998**, *93*, 411.
4. Hoops, S. C.; Anderson, K. W.; Merz, K. M. J. *J. Am. Chem. Soc.* **1991**, *113*, 8262.
5. Ryde, U. *Proteins* **1995**, *21*, 40.
6. Lu, D. S.; Voth, G. A. *Proteins* **1998**, *33*, 119.
7. Vedani, A.; Huhta, D. W. *J. Am. Chem. Soc.* **1990**, *112*, 4759.
8. Stote, R. H.; Karplus, M. *Proteins* **1995**, *23*, 12.
9. Wasserman, Z. R.; Hodge, C. N. *Proteins* **1996**, *24*, 227.
10. Darden, T. A.; York, D.; Pedersen, L. *J. Chem. Phys*. **1993**, *98*, 10089.
11. Roe, R. R.; Pang, Y.-P. *J. Mol. Model.* **1999**, *5*, 134.
12. Ryde, U. *Eur. Biophys. J.* **1996**, *24*, 213.
13. Rabenstein, D. L.; Daignault, S. A.; Isab, A. A.; Arnold, A. P.; Shoukry, M. M. *J. Am. Chem. Soc*. **1985**, *107*, 6436.
14. ElYazal, J.; Pang, Y.-P. *J. Phys. Chem. B* **1999**, *in press*.
15. Cornell, W. D.; Cieplak, P.; Bayly, C. I.; Gould, I. R.; Merz Jr., K. M.; Ferguson, D. M.; Spellmeyer, D. C.; Fox, T.; Caldwell, J. W.; Kollman, P. A. *J. Am. Chem. Soc.* **1995**, *117*, 5179.
16. Pogue, R. F.; Atkinson, G. *J. Soln. Chem.* **1989**, *18*, 249.
17. Frisch, M. J.; Trucks, G. W.; H.B., S.; Gill, P. M. W.; Hohnson, B. G.; Robb, M. A.; Raghavachari, K.; Al-Laham, M. A.; Zakrzewski, V. G.; Ortiz, J. V.; Foresman, J. B.; Cioslowski, J.; Stefanov, B. B.; Nanayakkara, A.; Challacombe, M.; Peng, C. Y.; Ayala, P. Y.; Chen, W.; Wong, M. W.; Andres, J. L.; Replogle, E. S.; Gomperts, R.; R.L., M.; Fox, D. J.; Binkley, J. S.; Defrees, D. J.; Baker, J.; Stewart, J. P.; Head-Gordon, M.; Gonzales, C.; Pople, J. A. *GAUSSIAN 94, revision D.4* Pittsburg, PA, 1995.
18. Xu, K.; Perola, E.; Kollmeyer, T. M.; Kaufmann, S. H.; Prendergast, F. G.; Pang, Y.-P. *J. Med. Chem.* **1999**, *in press.*
19. Boehm, T.; Oreilly, M. S.; Keough, K.; Shiloach, J.; Shapiro, R.; Folkman, J. *Biochem. Bioph. Res. Commun.* **1998**, *252*, 190.
20. Pearlman, D. A.; Case, D. A.; Caldwell, J. W.; Ross, W. S.; Cheatham III, T. E.; Debolt, S.; Ferguson, D.; Seibel, G.; Kollman, P. A. *Comput. Phys. Commun.* **1995**, *91*, 1.
21. Pang, Y.-P.; Miller, J. L.; Kollman, P. A. *J. Am. Chem. Soc.* **1999**, *121*, 1717.
22. Ryckaert, J. P.; Ciccotti, G.; Berendsen, H. J. C. *J. Comput. Phys.* **1977**, *23*, 327.
23. Berendsen, H. J. C.; Postma, J. P. M.; van Gunsteren, W. F.; Di Nola, A.; Haak, J. R. *J. Chem. Phys.* **1984**, *81*, 3684.
24. Jorgensen, W. L.; Chandreskhar, J.; Madura, J. D.; Impey, R. W.; Klein, M. L. *J. Chem. Phys.* **1982**, *79*, 926.
25. Cieplak, P.; Cornell, W. D.; Bayly, C.; Kollman, P. A. *J. Comp. Chem.* **1995**, *16*, 1357.